PONTIFICIA UNIVERSIDAD CATOLICA DE CHILE
ESCUELA DE INGENIERIA

DEVELOPMENT OF A BIOCOMPATIBLE POST-PROCESS FOR 3D-PRINTED CALCIUM SULFATE PARTICLES TO ENHANCE ITS PHYSICAL PROPERTIES

IGNACIA A. CANCINO

Thesis submitted to the Office of Research and Graduate Studies in partial fulfillment of the requirements for the Degree of Master of Science in Engineering

Advisor:
JOSÉ T. EGAÑA

Santiago de Chile, May, 2021

PONTIFICIA UNIVERSIDAD CATOLICA DE CHILE
ESCUELA DE INGENIERIA

DEVELOPMENT OF A BIOCOMPATIBLE POST-PROCESS FOR 3D-PRINTED CALCIUM SULFATE PARTICLES TO ENHANCE ITS PHYSICAL PROPERTIES

IGNACIA A. CANCINO

Members of the Committee:

JOSÉ T. EGAÑA ERAZO

JORGE RAMOS GREZ

ALEX VARGAS DIAZ

LEONARDO VANZI

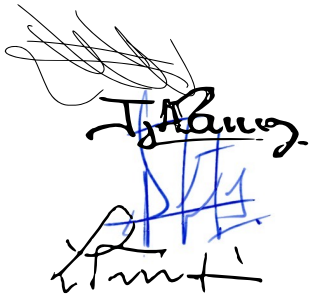

Thesis submitted to the Office of Research and Graduate Studies in partial fulfillment of the requirements for the Degree of Master of Science in Engineering

Santiago de Chile, May, 2021

To my parents, sister, family and friends.

ACKNOWLEDGEMENT

I would like to express appreciation to my thesis advisor José T. Egaña who accepted me in his laboratory with great enthusiasm and support. Without his help for adapting to difficult circumstances and continuous spirit of curiosity and adventure, none of this would have been done. He not only provided me with great innovative ideas to my research on but also supported me in my personal decisions like attending congresses (PIRO and PARADIGMA) and doing an internship in France for six months, which helped me broaden my curiosity and international relationships.

I would also like to thank the Geodbone team, in particular to Dr. Alex Vargas and Jorge Ramos, for making this work possible and sharing their knowledge, support, help and guidance throughout the course of the thesis. In addition, I want to acknowledge Leonardo Vanzi for his time in correcting this thesis.

I would also like to show my appreciation to Dr. Jovita Besa, who performed the scanning electronic microscopy (SEM) images, Dr. Pedro Bouchon, who provided me with the texture analyzer, MSc. David Ñecuñir, who helped me performed the cell culture experiments, cell staining and amazing visual illustrations. Also, to Miguel Miranda who shared his knowledge by teaching me about zebrafish care and helped me perform the zebra fish experiments.

Finally, I want to acknowledge my labmates and co-workers from the biomedical and biological institute at PUC who not only did they teach me different techniques and theoretical knowledge of biochemistry but also brought me lots of encouragement and positive attitude during the frustrating and challenging times.

GENERAL INDEX

Page

FIGURES INDEX

Page

APPENDIX INDEX

ABBREVIATIONS

3D printing	Three-dimensional printing
$CaCl_2$	Calcium chloride
Calcein AM	Calcein acetoxymethyl
DMEM	Dulbecco's Modified Eagle's
DMSO	Dimethyl sulfoxide
EM	Elastic modulus
Hpf	Hours post fertilization
LDH	Lactase dehydrogenase
microCT	Microcomputed tomography
PBS	Phosphate buffered saline
PI	Propidium Iodide
PMS	Phenazine methosulfate
SEM	Scanning electron microscopy
YS	Yield strength
w/v	Weight/volume
XTT	2,3-bis-(2-methoxy-4-nitro-5-sulfophenyl)-2H-tetrazolium-5-carboxanilide

RESUMEN

La ingeniería de tejidos óseos es una disciplina emergente que tiene como objetivo principal mejorar la regeneración a través del uso de injertos de hueso. La impresión 3D con sulfato de calcio es una herramienta que permite crear objetos a medida para distintas aplicaciones. El sulfato de calcio se puede utilizar como injerto de hueso dada su composición y su potencial de reabsorción. La impresión en sulfato de calcio tiene la desventaja que al imprimir objetos pequeños y/o delgados, estos son mecánicamente inestables por lo que no pueden ser implantados. Por esto, se busca desarrollar un post-procesamiento polimérico a base de alginato para estabilizar estos objetos. El alginato es un polímero biocompatible, vastamente disponible y permite la encapsulación de componentes.

Con el fin de procesar las partículas se realizó una cobertura de alginato a las partículas impresas a través de *cross-linking* con $CaCl_2$. Las propiedades mecánicas fueron medidas usando un ensayo de compresión uniaxial y la estabilidad fue medida a través de pruebas de solubilidad, superficie, grado de hinchazón e imágenes con microscopía electrónica de barrido para visualizar rugosidad. Posteriormente, se realizaron ensayos de biocompatibilidad *in vitro* e *in vivo*, utilizando la línea células NIH/3T3 y el modelo de larvas de peces cebra, respectivamente.

Los resultados de este trabajo muestran que el post-procesamiento de partículas de sulfato de calcio permitió estabilizarlas. Las pruebas mecánicas mostraron un aumento en el módulo elástico y la resistencia a la compresión para las partículas cubiertas con 2% de alginato. Las pruebas de solubilidad mostraron una disminución de 70% en la cantidad de sulfato de calcio en el medio, pero un aumento de 20% en su área. Además, el grado de hinchazón de la partícula procesada fue de 157%. Finalmente, los resultados muestran que la partícula procesada es biocompatible para las células NIH/3T3 y para las larvas de peces cebra a 48 horas de exposición.

Se evaluaron la mayoría de las propiedades necesarias para un injerto mecánicamente estable y biocompatible. Dejando abierta preguntas sobre el proceso de regeneración ósea como el añadir componentes bioactivos al alginato para mejorar su potencial terapéutico.

Palabras claves: sulfato de calcio, alginato, impresión 3D, ciencia de los materiales, ingeniería de tejidos, medicina regenerativa, regeneración ósea.

ABSTRACT

Bone tissue engineering is an emerging discipline whose main goal is to improve tissue regeneration through the use of bone grafts or scaffolds. Binder jettting 3D printing with calcium sulfate is a tool that has allowed tailor-made design for various applications. As calcium sulfate can be employed as a bone-graft due to its ceramic nature and reabsorption potential it is highly attractive to fabricate biomaterials out of it. This technology's limit is that small and thinner objects become brittle and turn to powder when handled. Thus, a biocompatible polymeric post-process is evaluated and performed with the use of calcium alginate. The polymer has been proven to be biocompatible, available, allows the encapsulation of components and particles and has bone grafting properties.

To create the post-processed particles an alginate coating was applied to the calcium sulfate particles through crosslinking with $CaCl_2$. The particles' mechanical properties were measured using a uniaxial compressive test on a texture analyzer. Stability of the resulting post-processed 3D printed particles was evaluated doing solubility testing (absorbance), normal area measurements, SEM imaging for surface roughness and degree of swelling. Also, toxicological assays have been performed with the use of NIH/3T3 cell line and zebrafish larvae model.

The polymeric coating was successfully performed on calcium sulfate particles as they did not break at touch. Mechanical testing showed increased young's modulus and compressive strength for the 2% w/v alginate coated particles and it was significantly different to the ones without coating. Solubility test showed 70% less calcium sulfate on medium after the coating process but with an increase of 20% in its surface area. In addition, the degree of swelling of the coated particle is about 258% or almost 2.6 times its weight. The particle is shown to be biocompatible to NIH/3T3 cell culture and to zebra fish larvae.

Most of the properties necessary for a mechanically stable and biocompatible bone scaffold are tested, and it opens questions on further research on the regeneration process and the possibilities of adding different components to the alginate coating to improve regeneration.

Keywords: calcium sulfate, alginate, 3d printing, material science, tissue engineering

1. INTRODUCTION

1.1 Bone tissue engineering

Tissue engineering is a concept that englobes the combination of a scaffold or matrix and cellular components creating an interface to be applied in the repair and regeneration of tissues (Venkatesan *et al.,* 2014). The main objective of tissue engineering is to go further on research and applications regarding organ transplants and material implantation (Langer *et al.,* 1993). Current tissue engineering strategies involve the use of different types of scaffolds that support cellular activity and whose main role is to repair, maintain and/or enhance regeneration on tissue defects (Martina *et al.,* 2007).

It is of great interest to improve the new methods on tissue engineering and particularly, in bone tissue engineering with the aim of cost reduction and less post-surgery trauma to the patients. Some of the clinical reasons to put efforts on the creation and development of innovative bone tissue engineering alternatives are the reconstruction and regeneration of large orthopedic defects and scaffolds or implants that can be more mechanically stable and lasting on the body (Burg *et al.,* 2000).

1.2 Bone grafts/scaffolds

In bone grafts, the gold-standard material is often the patient's own bone (autologous bone graft). This procedure has various limitations due to the low availability of donor sites of greater bone volume but also to the problems concerning an additional surgery injury, which is sometimes much more aggressive than the repairing the actual bone. To avoid these problems, various types of synthetic bone grafts have been developed. They are mostly composed of tri-calcium phosphate, hydroxyapatite, calcium sulfate and most of them are used as composites with other biomaterials (Pape *et al.,* 2010).

In order for a bone graft to be of successful implantation, it must require certain characteristics. It is known that osteoblast proliferation is sensitive to surface topography, strain or other mechanical stimuli. The aspect of a material will influence the bone or

fibroblastic differentiation of a tissue. Properties like particle size, shape, and surface roughness affect cellular adhesion, proliferation, and phenotype (Boyan *et al.,* 1996).

Applications of bone grafts in the clinical setting include spinal applications, fracture healing and filling bone defects. In these applications the bone graft must be modeled into the appropriate volume and shape of the defect and, in order for it to be of optimal use, the bone graft must be biodegradable (Khan et al., 2000).

1.3 Calcium sulfate 3D printing

3D printing technology comes in various shapes and sizes regarding the application. In particular, calcium sulfate is a low-cost material, which resembles the bone's inorganic chemical composition. It has also been previously used as a bone graft (Kumar *et al.,* 2013). One of the main problems of using calcium sulfate as a bone graft it is that it requires a dry environment to set and when exposed to wet environments it tends to soften and fragment. Thus, it has no reliable mechanical properties *in vivo* and it has limitations on its application (Moore *et al*., 2001).

3D printing with calcium sulfate is a technique that is more and more being recognized by the scientific community as it allows personalized and detailed object fabrication (Liu *et al.,* 2018). Ceramic-based scaffolds such as calcium sulfate, β-tricalcium phosphate and hydroxyapatite have been used as bone defect fillers as they are osteoconductive and can be resorbed at different degradation rates due to its similarity with the inorganic composition of bone (Laurencin *et al.,* 2006). One of the main challenges on the fabrication of ceramic-based biomaterials for bone tissue engineering is to get a desired shape and size specifically for an application. Thus, three-dimensional printing (3D printing) of ceramic-based bone grafts, such as calcium sulfate, has become an important manufacturing method to deal with creating a variety of designs and general structures (Aldemìr *et al.,* 2015). However, there are several complications in the fabrication of small size objects (less than 3 mm) because the pieces are usually so brittle that they lose their shape and mechanical strength in order to be useful of any kind.

ASTM F2792 defines binder jetting as “an additive manufacturing process in which a liquid bonding agent is selectively deposited to join powder materials.” (Mostafaei *et al.,* 2020). The following steps need to be performed to fabricate a binder jetted object (Allen *et al.,* 2000). First, a 3D design is required. Usually a CAD model is obtained with a desired shape to print. This is sequentially sliced into thin layers and saved a an STL file that can be used for printing. Then, a thin layer of powder is thrown over the building chamber and a counter-rotating roller spreads it evenly while also compacting lose powder. Then, a liquid binder solution (usually made of a water and alcohol mix) is placed in the printhead (similar to inkjet printers) and the binder is jetted onto the powder according to the directions of the CAD file. Then, the process repeats itself until the last layer of powder is printed. The printed powder chamber is left for a few hours so that the powder can settle and dry completely (Mostafaei *et al*., 2020). After this time, it is of common practice that the printed parts are moved to an oven for curing by heating to 180 to 200 °C for some time based on the volume and binder characteristics (Enneti *et al*., 2018).

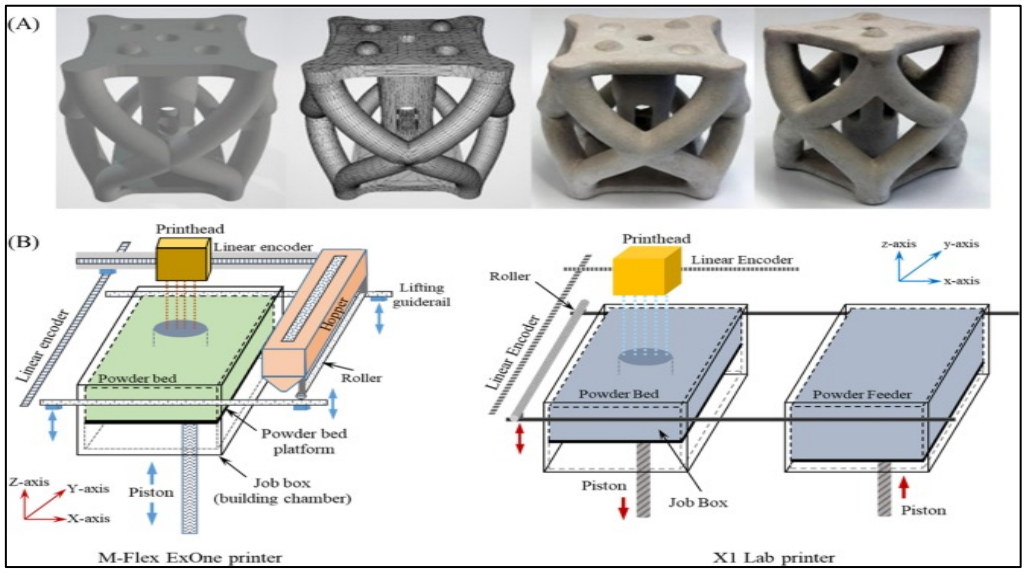

Figure 1: 3D printer technology. A) CAD file, STL file, and printed object. Image retrieved form (Ingaglio *et al*., 2019) B). Diagram of 3D binder jet technology with two types of powder feeding, (left) powders are supplied using a hopper, these are spread on the powder bed, and powder compaction is achieved using a roller tube and (right) a powder supply as a feeder in which a roller swipes powder on the powder bed on the top layer of the built area. Image retrieved from (Mostafaei *et al.,* 2020).

The second type of technology is commonly used where the binder is fed from the print head and the powder is supplied through a roller (figure 1, B). This ensures the formation of calcium sulfate particles already dried and with a desired shape given by the machine's user.

1.4 Polymers for mechanical stabilization of bone grafts

Bone tissue engineering solutions have included different components and polymers like demineralized bone matrix, collagen, calcium phosphate, polylactide, poly (lactide-co-glycolide), polylactide-polyethylene glycol, hydroxyapatite, dental plaster, titanium, etc. (De Groot *et al.,* 1998; Tsuruga *et al.,* 1997).

When speaking about polymers, they can differ in many properties (for example: molecular weight, surface and thermal transitions), which translates in different qualities like absorption rates, phenotype and cellular adhesion to a surface. (Hollinger *et al.,* 1997). It is also important to notice that tissue responses to polymers *in vivo* depend on biocompatibility and degradative by-products of the polymer (Hollinger J. B. *et al*., 1986) as well as, on the environment of the site where the polymer will be applied (like oxygen and pH levels) (Boyan *et al.,* 1996).

One of the most used polymer for bone graft are the poly (lactide-co-glycolide) matrices. They can be porous, be customized to a desired absorption time, and they are biocompatible (Mikos *et al.,* 1994). Another polymer used in bone graft 3D printing is collagen. In a study collagen was dissolved into the binder solution to fabricate collagen-calcium phosphate composites, claiming to reduce the viscosity and surface tension through a heat treatment while being adequate for its use as a bone graft (Inzana *et al.,* 2014).

Then, there is calcium alginate, a polysaccharide which is extracted from brown algae. It is a proven biocompatible polymer with vast applications in medicine, including the delivery of drugs, tissue scaffolds and also for human consumption. Its mechanical, chemical and rheological properties have been a key factor in choosing alginate for tissue

regeneration (Felfel *et al.,* 2019). In addition, is suitable to be in contact with biomolecules such as proteins and nucleic acids, and also for living cells, such as islets of Langerhans (Pawar *et al.,* 2012). In order to form a hydrogel, alginate undergoes a crosslinking reaction with divalent cations such as Ca^{2+}, Mg^{2+}, Ba^{2+}, and Sr^{2+} and this allows it to be a low-cost hydrogel (Lee *et al.,* 2001). Alginate crosslinked with calcium ions can be utilized in tissue engineering. The calcium crosslinked alginate hydrogels showed increased differentiation and proliferation of the rat bone marrow cells depending on calcium composition (Wang *et al.,* 2003). The concentration of calcium ions and other components, such as cells, play an important role in physical properties and gelation behavior of the prepared gels (Rajesh *et al.,* 2017). An *in vivo* study showed that alginate hydrogel prepared by combination crosslinking method (using calcium ions and cells) was useful in cartilage tissue engineering (Park *et al.,* 2009).

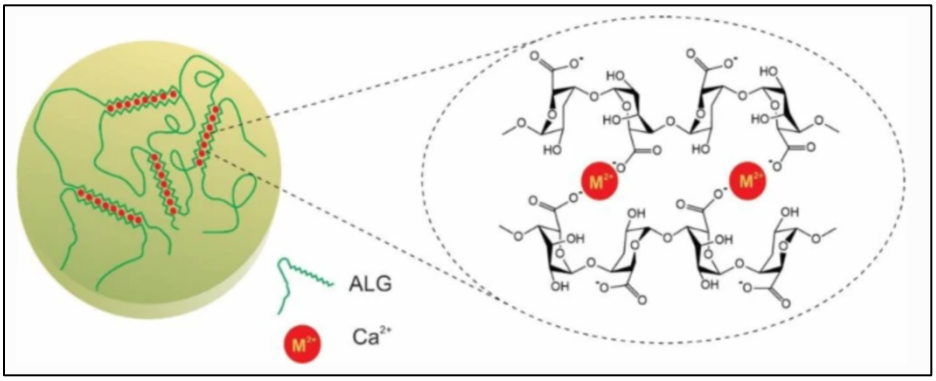

Figure 2: Diagram of alginate crosslinking with calcium ions. Calcium ions bind to the free electron of oxygen form each monomer creating an egg-box pattern. ALG= alginate; M^{+2} = divalent cation. Image retrieved from (Abasalizadeh *et al*., 2020)

For all the reasons mentioned above, it is of special desire to test alginate as a biocompatible stabilizing hydrogel coating for the calcium sulfate 3D printed particles. As it allows not only the physical stabilization of bone grafts but also it aids in bone regenerating purposes.

1.5 Mechanical testing

Mechanical stabilization is an important property for bone grafts as it ensures that the bone graft will perform properly during *in vivo* tissue regeneration (Lanza *et al.,* 2020). It is also of great importance to do compression tests to the bone grafts/scaffolds as they would be constantly manipulated and pressed by the surgeons.

Specifically, it is required to increase the elastic modulus and yield strength of the alginate-coated particle and compare it to the initial calcium sulfate only particles. The elastic modulus measures the resistance of a material to elastic deformation. It is computed as the linear slope of a stress-strain plot. In the case of porous materials or material in which their geometry involves empty space in between, the elastic modulus is given by the first linear slope of the plot and it is much lower than non-porous materials (Lu *et al.,* 1999). Yield strength, which is defined as the maximum strength a material can hold before it enters plastic deformation is an important property of bone grafts. This value is taken as the maximum normal stress it takes for the material to be flattened, and so it is computed as the maximum value of the first linear part of the stress-strain plot. Both of these properties can be obtained from a strength vs strain plot (figure 3). Where the object is compressed at a constant rate (mm/s) until it reaches a maximum distance it can compress.

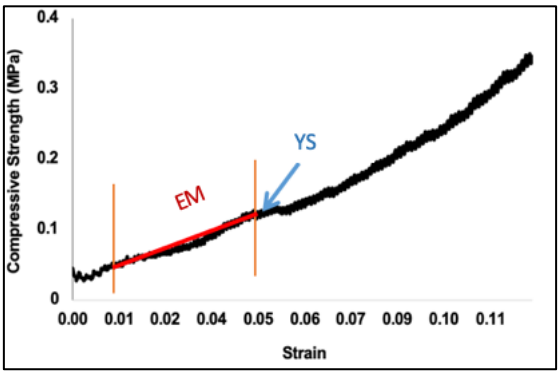

Figure 3: Replicate of a stress-strain curve for a single 2% w/v alginate coated particle. EM= Elastic modulus; YS= Yield strength. The elastic modulus is taken as the first linear slope of the plot.

When compressing a group of particles in a confined recipient, the elastic modulus that is computed on the stress-strain is not the real elastic modulus of the material but it represents a more porous material conformed of many particles whose geometry allows them to form spaces between them or "pores".

1.6 Physical stabilization and characterization

Not only mechanical properties are important to measure to ensure that the application of a scaffold or bone graft is not failing its purpose of being applied into live tissue. Solubility in physiological conditions ensures that at least for a few days, the bone graft will maintain their integrity and shape after being applied and thus it is an indicator of stability. In addition to this, scanning electron microscopy (SEM) images aid to visualize in-depth images of the surface roughness, porosity and morphology and how any process done to the scaffold changes it.

Another important property is swelling. Swelling is the capacity of a hydrogel (in this case alginate) to absorb water or physiological solutions. Swelling can be measured by looking at the change in weight in dried and wet conditions. The degree of swelling can be measured with the following expression (Severino *et al*., 2015).

$$Degree\ of\ Swelling\ (\%) = \frac{M_{water}}{M_{material}} \cdot 100$$

Moreover, the morphology of a scaffold is important as it conditions the environment for tissue regeneration. It has been reported that even with the same chemical composition, the geometry of a ceramic scaffold can produce different expression of phenotype markers. Where bone grafts with structures exhibiting subcellular microstructures were more osteoinductive than the ones that were not (Ratner *et al.,* 2004).

1.7 NIH/3T3 *in vitro* biological model

In vitro models allow testing biocompatibility with higher reproducibility and less cost than more complex biological models for testing scaffolds or bone grafts, such as minor mammals. Some advantages of *in vitro* testing are the ability to control the conditions of

cell growth and development and also to measure the response of the cells when exposed to a particular agent. *In vitro* testing proves to be fast, affordable and sensitive in order to make repetitive measurements a testing variable (Olivier *et al*., 2012).

Testing biocompatibility in a standardized cell line, turns out to be stable and reliable for toxicology studies. The standard mouse fibroblasts (NIH/3T3) is widely used for biocompatibility (cytotoxicity and viability) testing as they are standardized. The use of other cells like osteoblasts as an *in vitro* model has some disadvantages as they are obtained from primary cell cultures and it can vary greatly depending on the individual they were taken from.

1.8 Zebrafish larvae model for toxicology tests

Finally, *in vivo* models are used to test the toxicity of the particle under a larger organism. The main reason of testing the particle (or other drugs) in *in vivo* models is that many drugs, shown to be safe in cell culture, prove toxic in larger animal testing. An effective *in vivo* study early on can reduce the number of drugs or compounds that go forward into larger animal testing (Parng *et al.,* 2005). The advantages of using zebrafish for drug screening or toxicity studies are mainly that they are small, affordable to maintain and can breed easily in large numbers. A single spawning from one couple of zebrafish can produce 100–300 eggs if maintained in the right conditions. The larvae with a size of only 1–4-mm long, can live for seven days in a single well of a standard 96-well microplate supported with the right medium (E3). (McGrath *et al.,* 2008).

Also, the zebrafish larvae model allows for the absorption of small molecules that are present in the surrounding water or medium through their skin and gills. This comes in great use for toxicology testing. Larger components in the medium can be delivered orally after this stage because zebrafish larvae begin to swallow at 72 hours post fertilization (hpf). When compared to testing with different animal models, statistically significant numbers of zebrafish can be used for each assay. Another important quality is that the transparency of zebrafish enables *in vivo* observation of live organisms and can also allow

the real-time observation of different stains, fluorescent tracers, antibodies, etc. (McGrath *et al.,* 2008).

2. HYPOTHESIS AND OBJECTIVES

2.1 Hypothesis: A post-process allows the 3D printed calcium sulfate particles to stabilize mechanically and morphologically while being biocompatible for medical applications.

2.2 General objective: To stabilize 3D printed calcium sulfate particles with a biocompatible post-processing.

2.3 Specific Objectives

Specific objective 1: To compare different approaches and define a protocol for stabilizing 3D printed calcium sulfate particles.

Specific objective 2: To characterize the stabilized 3D printed particle in terms of mechanical, physical and morphological properties.

Specific objective 3: To study the biocompatibility of the stabilized particles *in vitro* and *in vivo*.

3. MATERIALS AND METHODS

3.1 3D printing and curing

The designed shape and dimensions of the objects (Patent pending PCT/CL2018/050066) were uploaded to 3D studio (Autodesk®). The objects were then printed using the zp®131 powder (mostly calcium sulfate) with the use of VisiJet® C4 Spectrum Clear binder by the Projet 160 printer by 3D systems. The particles had approximate dimensions of 2.4 mm x 1.9 mm x 0.7 mm each with a geodesic shape. After printing they were left on the machine to dry for 24 hours. Then, they were heated at 200ºC for 15 minutes to cure and dry completely (Enneti *et al.,* 2018).

3.2 Ammonium phosphate ion exchange

Ion exchange was performed using three solutions of $NH_4H_2PO_4$ at different concentrations (1M, 2M and 3M). All of them were diluted in distilled water. Three calcium sulfate particles were added to each tube containing 500 µl of the respective solutions. Protocol was followed as previously described in literature (Lowmunkong *et al.,* 2007).

3.3 Calcium alginate coating

Different weight volume (w/v) concentrations of alginic acid sodium salt solution (PanReac, AppliChem Gmbh, Darmstadt, GE) with distilled water were made (0.04%, 0.4%, 2%, 4%). The concentrations were chosen due to the maximum solubility concentration we could obtain (4%) and diluted them 10 and 100 times. Then, a 10% calcium chloride ($CaCl_2$) solution was made with distilled water, as previously described (Hornyák *et al.,* 2017).

To coat each particle, they were handpicked one by one with a measuring spoon and they were submerged in the alginate solution for 60 seconds. Then, they were placed in thin paper towel to allow excess alginate to be absorbed. After this, they were completely dipped in the calcium chloride solution for 60 seconds. The particles then were washed

and rinsed three times with distilled water and dried at 60 ºC for more than 3 hours. The particles were then kept at room temperature in air tight compartments until they were ready to be used. For cell culture testing, a higher purity sodium alginate was used at 2% w/v (PROALG, Commercial ABO Ltda., Chile).

3.4 MicroCT imaging

Microcomputed tomography (microCT) images of alginate covered particles was performed using SkyScan 1272 micro-CT (Bruker, MA, USA). The volume of the sample was given by a 1 ml centrifuge tube and the actual sample size was around 500 µl. Reconstruction of 3D images was performed by the microCT unit of the Department of Chemical and Bioprocess Engineering using the CTAn (CT-Analyzer) software (Bruker, MA, USA).

3.5 Mechanical testing

Elastic modulus and yield strength of single particles were measured using the texture analyzer TA.XT plus by Texture Technologies® with the use of a flat piston with 10 mm width length and the maximum force was 30 kN. The tests were repeated at least 9 times of each group and the particles were placed facing downwards (convex side up). The contact area was calculated as an approximation of the surface projection of the particle on the x-y plane and so the rectangular area was used to obtain compression strength (2.37 mm x 1.90 mm). For measuring the mechanical properties of groups of particles, two different conditions were analyzed: 2% alginate (n=7) and without alginate (n=11). The samples contained 0.5 ml of particles and were placed in a cylindrical probe of 11 mm. The area of compression was 10 mm and it was compressed 2 mm deep (about 34% of compression). The speed of the test was 0.5 mm/sec for both single and grouped samples. The original data was analyzed with Microsoft EXCEL®. To obtain elastic modulus and compression strength (YS), the first linear section of the plot was analyzed. Elastic modulus was obtained as the slope of the line and compression strength was obtained as the higher value of the line before it enters elastic deformation. The outlier points were removed as manipulation of the particles was difficult and some of the particles were not

in correct position. One-way ANOVA and Mann-Whitney test were performed with GraphPad Prism version 7 software.

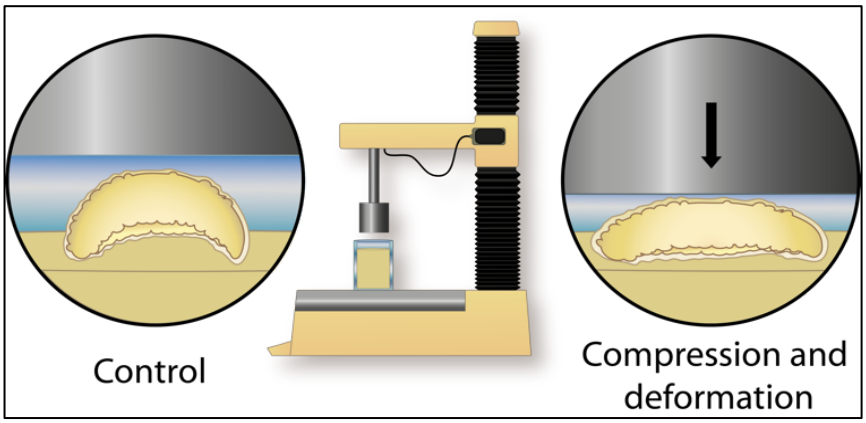

Figure 4: Compression test diagram of single particle. Diagram display of the compression test performed to each individual particle. The particles were placed with their convex side up, as shown in the figure.

3.6 Solubility in physiological conditions

Relative solubility of the post-processed particle was measured by allowing 3 particles (2%) be submerged in 2.5 ml of PBS 1x solution at 37ºC for 7 days (n=3). The control samples were 3 non-coated particles with the same treatment. After the seven days, microscopy photographs were taken for both groups and the supernatant was taken using a micropipette without touching the bottom of the plate. Absorbance was measured at 500 nm with the use of EPOCH™ microplate spectrophotometer. Statistical analysis done with unpaired t-test with Welch's test correction with the use of GraphPad Prism version 7 software.

3.7 SEM imaging

Scanning electron microscopy (SEM) images were taken of three different particles before and after the calcium alginate coating. The particles were dried and covered with a gold coating. They were observed at different microscopic augmentations using a backscattered electron detector. Images were taken with a scanning electron microscope Hitachi TM3000 (Hitachi High Technologies Inc., Tokyo, Japan) and processed using the

software provided by the brand at the Advanced Microscopy Unit from Pontificia Universidad Catolica de Chile.

3.8 Swelling degree

Weight was measured in groups of ten particles and repeated ten times per group using an analytical scale. Three different groups were weighted (no polymeric coating, 2% polymeric coating and wet 2% polymeric coated particles). The standard deviation and mean were computed from the data. Free volume (air) was computed by adding distilled water to dried particles until they reached a total of 100 μl in a measured microcentrifuge tube. Then, they were weighted and the wet particle volume (computed previously for 11 particles approximately) was subtracted from the total amount. Statistical analysis done with Mann-Whitney test with the use of GraphPad Prism version 7 software.

3.9 Particle area quantification

In order to observe and measure how much of the original shape of the particle was changed due to the alginate coating process, images were taken from 20 different particles before and after the alginate coating using a stereo zoom microscope (Leica Microsystems, Wetzlar, Germany). The images were process with ImageJ 1.x software (ImageJ, MD, USA) to compute the initial and final area. Statistical analysis done with Mann-Whitney test with the use of GraphPad Prism version 7 software.

3.10 Cell culture for viability and toxicological assays

NIH/3T3 mouse fibroblasts were cultured in DMEM medium (Mediatech Inc., Manassas, VA, USA) supplemented with 10% fetal bovine serum (PAN Biotech, UK) and 1x concentration of penicillin/streptomycin (Biological Industries, Connecticut, USA) and were kept in an incubator at 37 ºC and 5% CO_2. About 50,000 cells were seeded in 24-well microplates. Cells were left to grow until they reached 70% confluence. Then, for every well 1 alginate-coated calcium sulfate particle was added (2% alginic acid using medical grade alginic acid) and left co-cultivated with the cells for 24 and 48 hours. As a viability positive control, the same number of cells were seeded but no particle was added.

As a death control, the same number of cells were used but 1% Triton X-100 was added for 20 minutes. For every condition, three replicates were done and the results were evaluated twice.

3.11 XTT viability assay

Cell viability was measured using the XTT assay (Invitrogen, CA, USA). After the incubation time of 24 and 48 hours, each well was incubated with 125 µL of a XTT/PMS solution in DMEM medium for 1 hour and a half at 37 ºC. Then, the supernatant of each well was taken and absorbance at 450 and 650 nm was measured using the EPOCH2 microplate reader (BioTek Instruments, Inc; Winooski, VT, USA).

To measure a percentage of viability, the background solution (no reagent) is sustracted from the sample measurement and the negative control. Then, the normalized sample measurement is divided by the negative control and multiplied by one hundred. According to the following expression where both absorbances are already normalized:

$$\text{Viability } \% = \frac{\text{Norm. Sample}}{\text{Norm. Negative Control}} \cdot 100\%$$

3.12 LDH toxicity assay

Cytotoxicity was measured with the use of Pierce LDH cytotoxicity assay kit™ (Thermo Fisher Scientific, Rockford, IL, USA), according to manufacturer's instructions. Briefly, after the incubation time (24 and 48 hours), the supernatant medium was taken from every well. 50 µL of the reaction mix from the kit was added to 50 µL of medium, they were thoroughly mixed and left at room temperature for 30 minutes. To stop the reaction, 50 µL of the Stop Solution was added. Then, absorbance was measured at 490 and 680 nm with the use of the EPOCH2 microplate reader (BioTek Instruments, Inc; Winooski, VT, USA). In order to compute a percentage of cytotoxicity, the sample absorbance at 680 nm (background absorbance) is subtracted from the absorbance at 490 nm (reaction absorbance) to get a normalized absorbance. To measure the cytotoxicity percentage the following equation was applied:

$$\text{Cytotoxicity } \% = \frac{\text{Norm. Sample} - \text{Norm. Neg. Control}}{\text{Norm. Pos. Control} - \text{Norm. Neg. Control}} \cdot 100\%$$

Where the sample normalized absorbance is subtracted from the normalized negative control (live cells) and divided by the subtraction of the positive control (death) and negative control (dead cells).

3.13 Calcein AM and PI live/dead assays

To test this, 50,000 NIH/3T3 cells were seed over glass covers and incubated with 1 particle for 0, 24 and 48 hours. The negative control (cellular death) were cells incubated with 1% Triton X-100 for 20 minutes. After the incubation time, the cells were incubated with calcein AM dye (3 µM) and PI (2.5 µM) in PBS buffer Ca^{2+}/Mg^{2+} (1 mM) for 30 minutes at 37 ºC. Images were taken with an epifluorescence microscope (Axio Observer Z1/7, ZEISS) and processed with the Zen Blue 3.0 software. Statistical analysis was done with GraphPad Prism (GraphPad Software, Inc., La Jolla, CA, USA). Statistical significance was determined with ANOVA test and multiple comparison was performed with Bonferroni test.

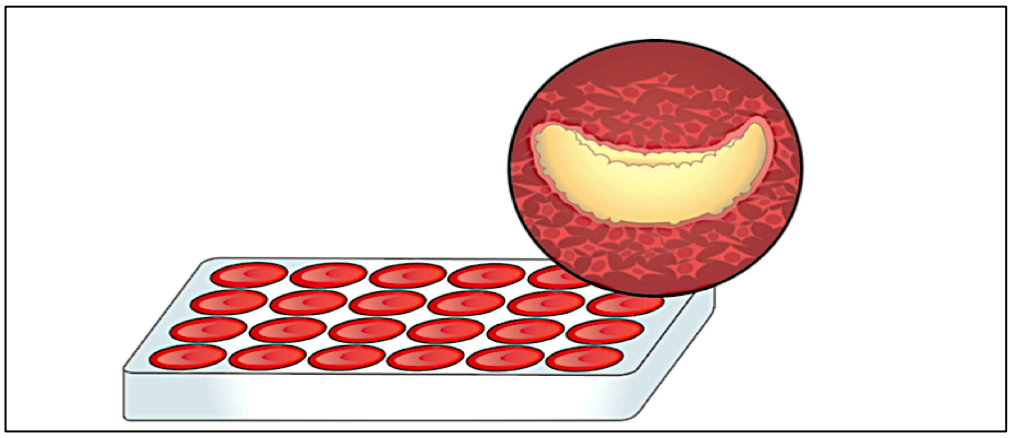

Figure 5: Diagram of viability and toxicity assays consisting on NIH/3T3 cells co-cultivated with particles. The diagram shows the *in vitro* experimental setting to evaluate biocompatibility. The seeded cells were at 70% confluence after adding a particle to each well. The different assays (XTT, LDH, Calcein AM and PI) were performed for each time (0, 24 and 48 hours). A positive control was used consisting in only cells and no particle. The magnification image shows an example of how the particle was displayed inside the wells.

3.14 Zebrafish breeding

For these experiments TAB5 zebrafish embryos were used. The fish were kept in tanks at 28 ºC, with water pH of 7 - 7.5, dissolved oxygen 7.8 mg/L and water conductivity of 500 – 600 uS. Feeding was done from Monday to Friday, twice a day at 9:30 a.m and 15:00 p.m. and Saturday, Sunday and holiday it was done once at 15:00 p.m. The fish were fed with dry granulated food (Gemma Micro 300/500, Skretting, ME, USA). The fish pairs were bred during the week. The fish pairs were kept in individual tanks with a breeding barrier at 18:00-19:00 hours. The next day at 9:00 a.m., the breeding barrier was lifted. Embryos were collected at noon of the same day, to avoid stress to the fish. Finally, the embryos were washed with E3 medium (5 Mm NaCl, 0.17 mM KCl, 0.33 mM, CaCl2, 0.33 mM MgSO4, pH 7.0) and methylene blue and were kept at 28 ºC in an incubator.

3.15 Zebrafish larvae toxicity assay

To obtain the zebrafish larvae, 120 zebrafish fertilized embryos (TAB5 strain) were picked and left in incubator at 28 ºC for one day or until they hatched. After this time, 4 days was awaited in order for the larvae to develop completely. Each day the E3 medium was changed from each dish and replaced by new medium. Then, ten zebrafish larvae were placed in each well of a 6-well plate and 5 ml of E3 medium was added respectively. The experiment once by triplicates. One is 10 particles coated with 2% alginate, as described in section 3.3, and the other is the positive control (no particles). The larvae were monitored for 24 hours and 48 hours. After the corresponding time, the zebrafish larvae were taken to the microscope and observed for heartbeats and they were counted as dead or alive accordingly. Then microscopy photos were taken using 1% low-melt point agarose and a representative larva for each condition.

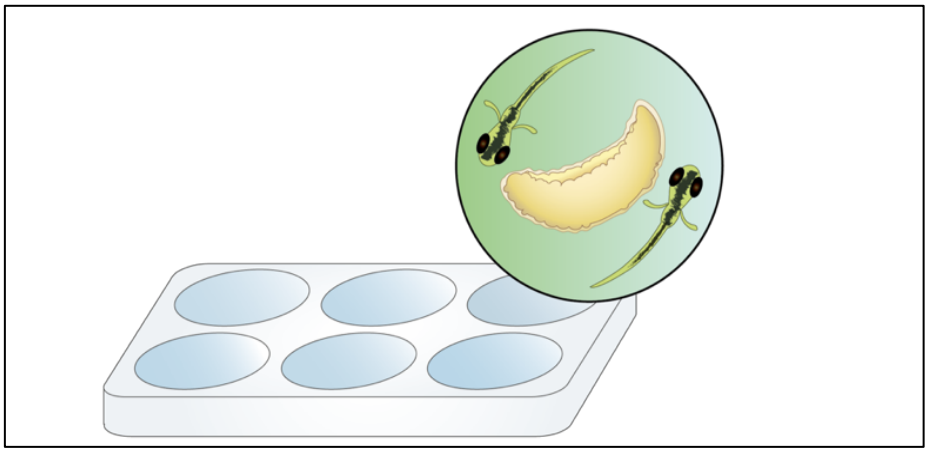

Figure 6: Zebrafish larvae experimental diagram. The diagram shows the *in vivo* experimental setting to evaluate biocompatibility. Ten larvae were seeded with ten particles in each well. Viability signs like heart beats were checked for each time (0, 24 and 48 hours). A positive control was used consisting of only larvae and no particles. The magnification image shows an example of how the particle was displayed inside the wells.

.

4. RESULTS

4.1 3D printing and processing

The calcium sulfate particles were successfully printed according to the original geodesic design. They did not turn black when curing them at 200 ºC for 10 minutes. However, they were still brittle to touch and difficult to handle as shown in the outside borders of the figure below and some turned into a beige color (figure 7). As the process allows evaporation of left over liquids, this curing step was maintained for all the following tests.

Figure 7: Calcium sulfate 3D printed particles after being heated. Left) Image shows the original particles after being printed and cured with heat. Scale 6 mm. Right) Zoom of the image. Scale 3 mm.

4.2 Ion exchange process

The ion exchange protocol was chosen as a way to increase mechanical properties by converting calcium sulfate to hydroxyapatite. As mentioned in materials and methods section, the already heated particles were submerged in ammonium phosphate

solutions. After the ion exchange reaction, it was observed that the particles lost their shape and formed a paste in the bottom of the microtubes (figure 8).

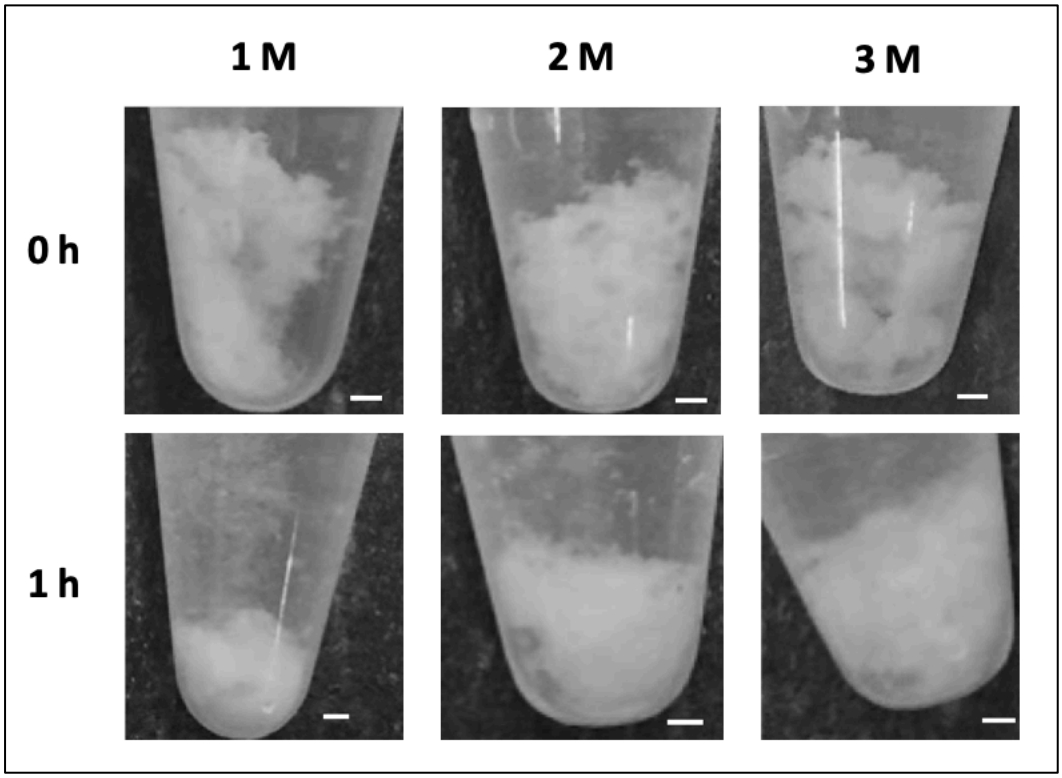

Figure 8: Ammonium phosphate ($NH_4H_2PO_4$) ion exchange reactions at different molar concentrations. First row) Particles submerged at 0 hours at the different molar concentrations, before the process. Second row) Particles submerged after 1 hour and 80 ºC at the different molar concentrations. Scale 1 mm.

It can be noted that the liquid solution did not have the necessary viscosity in order to prevent the particles from dissolving. The particles immediately collapsed to the bottom of the microtube when in touch with the solution forming a mud-like lump and it completely lost its shape. Then, after one hour of incubation in the solution, the particles kept collapsing in the bottom of the microtube totally destroying its original shape. For this reasons, this protocol was discarded for morphological stabilization purposes.

4.3 Calcium alginate coating process

A different approach was tested using alginate as a way to coat and stabilize the particles. From all the groups that were submerged in the first alginic acid solution, only the 0.04% w/v group was completely dissolved and lost the shape. From the other groups, there was no observable difference between the conditions (0.4%, 2% and 4%). Still, it was slightly more difficult to prepare the 4% as it becomes thick enough that it takes longer to dissolve the alginic acid in water. Also, regarding the 0.4% solution it was seen that the particles are more likely to deform when submerging them comparing to the 2%.

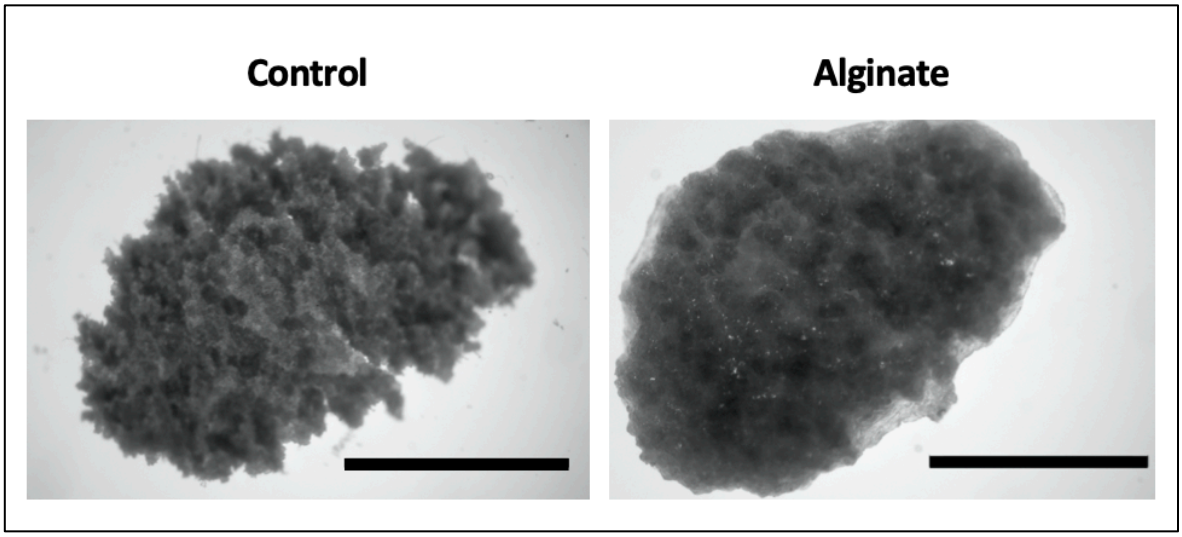

Figure 9: Change of morphology of a single particle before and after the polymeric process (dried). Left) Control: Before alginate coating. Right) Alginate: Particle with 2% alginate coating. Scale of 2 mm each.

The images show that the coating makes the rough edges of the calcium sulfate particles smoother.

4.4 Mechanical properties of single particles

The compression of single particles was repeated 9 times for each condition. From the stress-strain curves we obtained the initial slope value and the compression strength at

which this slope ends. The results from the mean and standard deviation of these measurements are shown below.

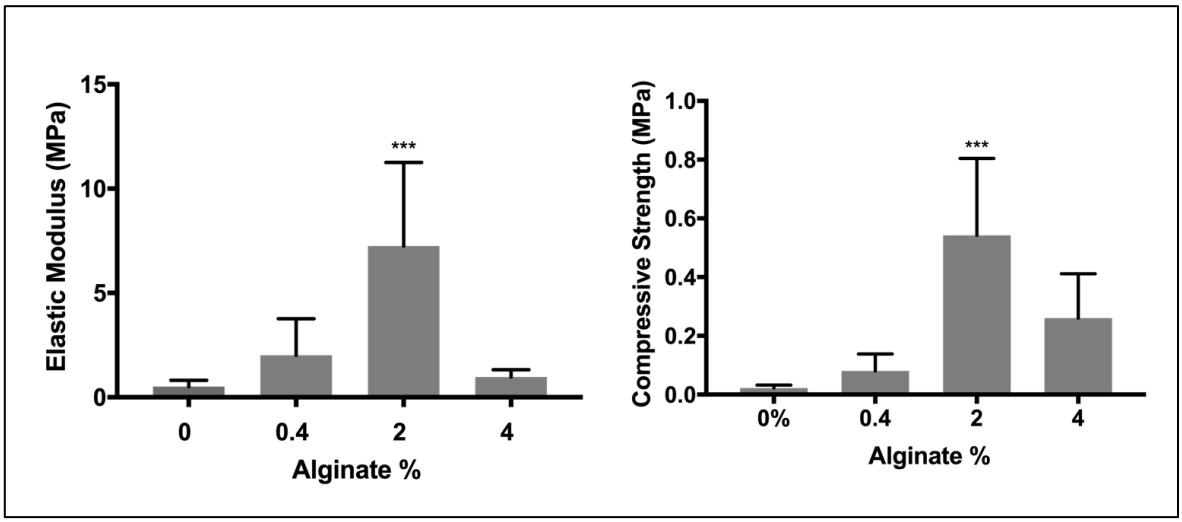

Figure 10: Measurements of mechanical properties at different concentrations of single post-processed particles. Left) Elastic modulus and right) yield strength of single particles processed with 0%, 0.4%, 2% and 4% alginate (n = 9). Statistical analysis done with one-way ANOVA and Tukey's multiple comparison test (*** $p < 0.001$).

It can be observed a large variation between groups in some conditions (2% vs. 4% alginate). It can be seen from the bar plots that 2% is the condition with higher elastic modulus and yield strength and is also significantly higher than the pre-processed particle.

Following these results, 2% alginate coated particles were chosen for following characterizations and from this section on this condition will be addressed as "alginate".

4.5 Area variation

In order to test how much of the particle area changes due to the alginate coating process, images of the same particle with its convex side up were taken before and after the process. After the quantification done with ImageJ software, we can observe that it does change the magnitude of the normal surface size, increasing 20.8%.

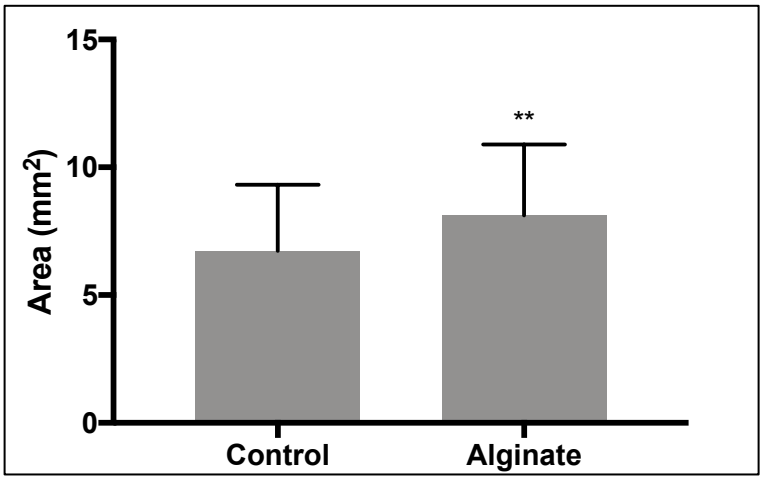

Figure 11: Quantification on the change of morphology of a single particle before and after the polymeric process (dried). Measurement of the top surface area (convex side up) in cubic millimeters before (control) and after alginate coating (2% alginate). Statistical analysis done with Mann-Whitney test (** $p < 0.01$).

4.6 Solubility testing

It was observed from the solubility test images (figure 12), that the alginate coating managed to keep the calcium sulfate particle in place which is shown as a transparent film surrounding the right picture.

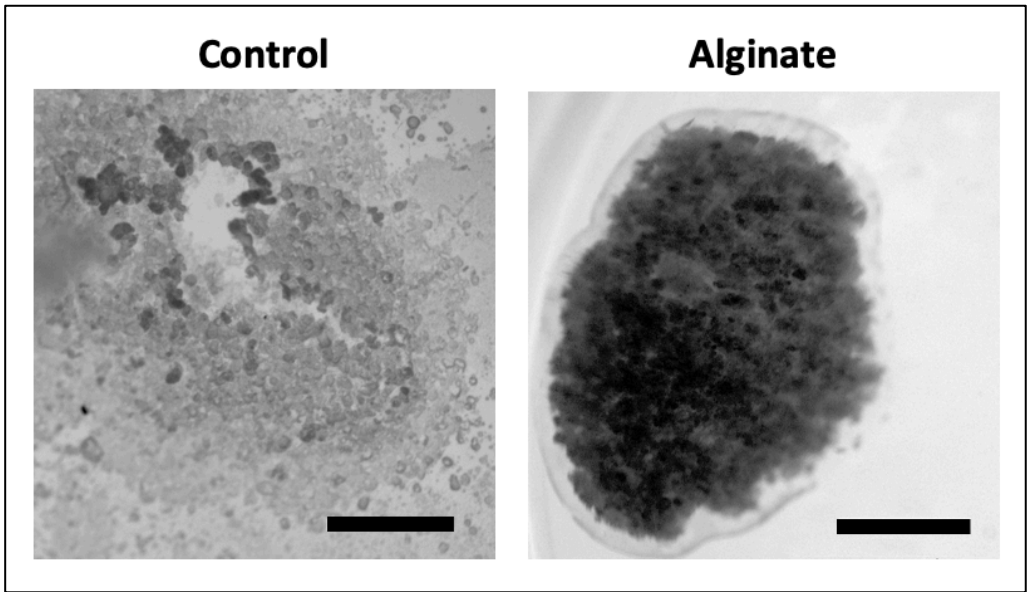

Figure 12: Stability under physiological conditions of the post-processed particle. Left) Control: particle without alginate coating. Right) Alginate: Particle with the 2% alginate coating. Scale 1 mm.

Then, the absorbance measurements showed that when the alginate coating was not added, the particle dissolved in the PBS buffer creating an opaque solution which resulted in higher light absorbance (500 nm for calcium sulfate). In contrast, when coated with alginate, the particles seemed to be retained and did not liberate as much powder into the solution resulting in a lower absorbance number. The absorbance numbers were converted into relative solubility percentage to explain this property better, where the absorbance of the 0% alginate group (non-coated) was taken as the 100% of solubility and the 2% alginate group was taken in relation to the non-coated one.

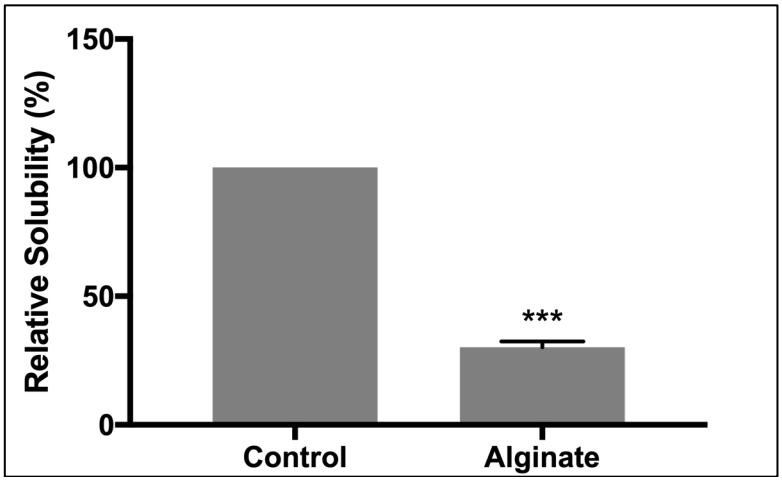

Figure 13: Relative solubility as a percentage of calcium sulfate on PBS solution when no alginate coating is added. The left column indicate the maximum calcium sulfate powder in solution for this shape. The right column indicates the percentage of calcium sulfate relative to the control (no alginate) that leaks into the solution, 30.21% of the control. Statistical analysis done with unpaired t-test (*** $p < 0.001$).

The results show that the alginate coated particles had significantly lower solubility in PBS medium with respect to the non-coated particles, thus decreasing about 69.79% of the calcium sulfate loose powder in solutions.

4.7 SEM images of the resulting particles

In order to visualize the roughness of the particle surface with and without the alginate coating, SEM images were taken (figure 14).

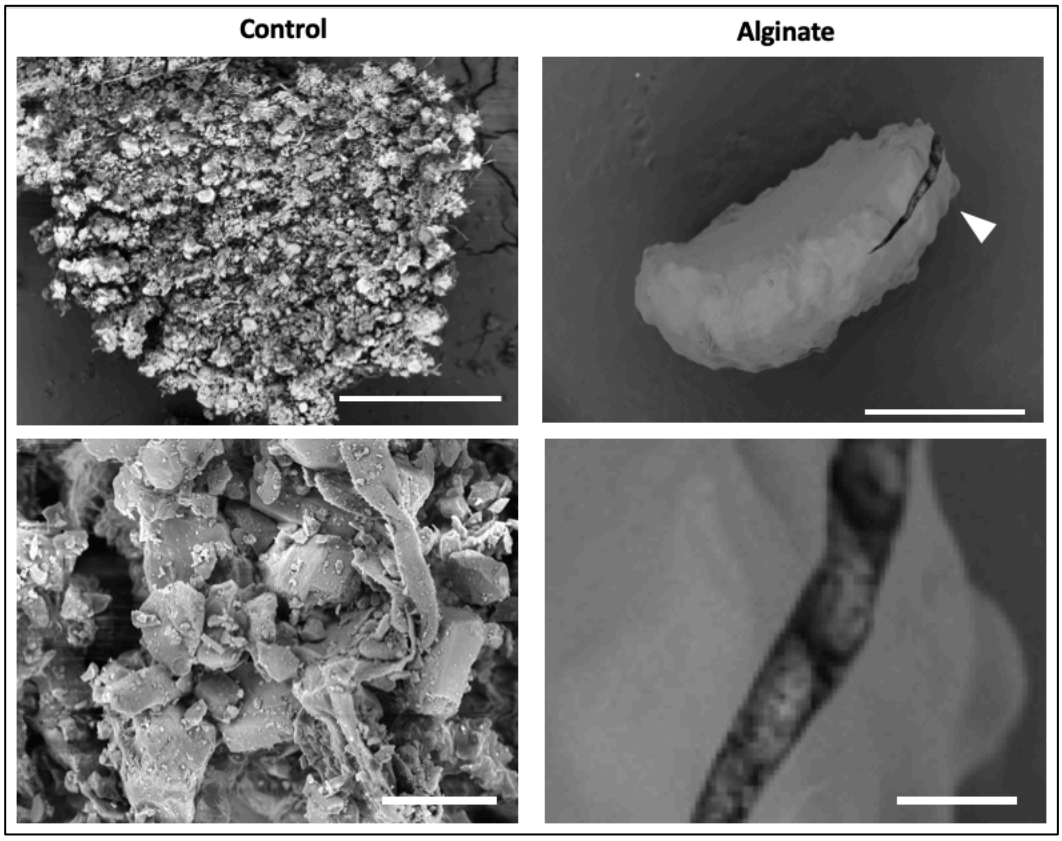

Figure 14: SEM imaging of the calcium sulfate particles, with and without the polymeric coating. Left) Control: Particle without the coating. Up) Surface of the particle without alginate. Scale 1 mm Down) Magnification on another non-coated particle. Calcium sulfate crystals can be observed. Scale 50 μm. Right) Particle with the 2% alginate coating. Up) A crack is observed on the edge of the particle. Scale 1 mm. Down) Zoom-in on the particles' surface and opening (where the arrow indicates). Calcium sulfate appears on the opening. Scale 125 μm. Images courtesy of J. Besa (Faculty of Medicine, PUC).

It can be observed that the particle with the alginate coating is much smoother that the non-coated but it seems to be less porous. In addition, calcium sulfate crystals can be observed at high resolution, showing a natural porosity of the material. Also, it can be seen that particles can have small defects on the alginate coating, showing that the alginate coating does not cover the particle perfectly and calcium sulfate can be exposed to the medium.

4.8 Swelling

The swelling effect of the coated particles was characterized by measuring the weight of the single particles. Here, we see a comparison of both groups of coated particles (dried and wet).

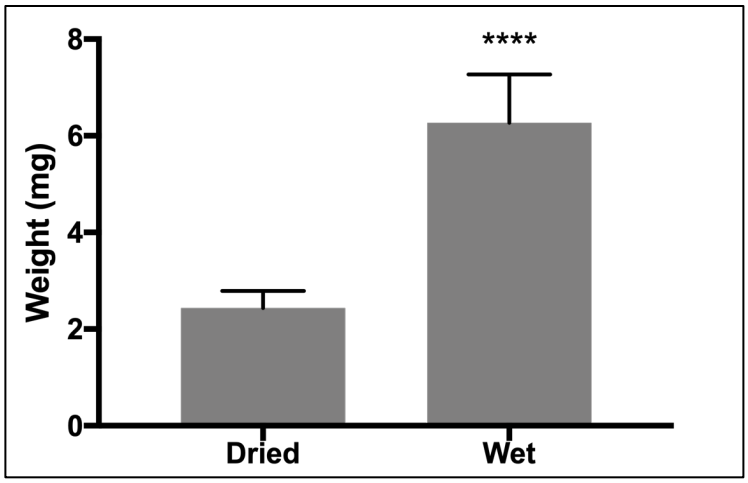

Figure 15: Characterization of mass before and after the process. Comparison of single-particle's weight with 2% alginate when dried and when wet (n=10). Statistical analysis done with Mann-Whitney test (**** $p < 0.0001$).

The particles had a degree of swelling of 258%, according to the average weight of each group. The difference between weights was significant.

4.9 Group behavior

An image of the 2% alginate coated particles with the polymeric post process is shown below. It can be seen that after the treatment the particles keep most of their original shape, leaving empty spaces in between.

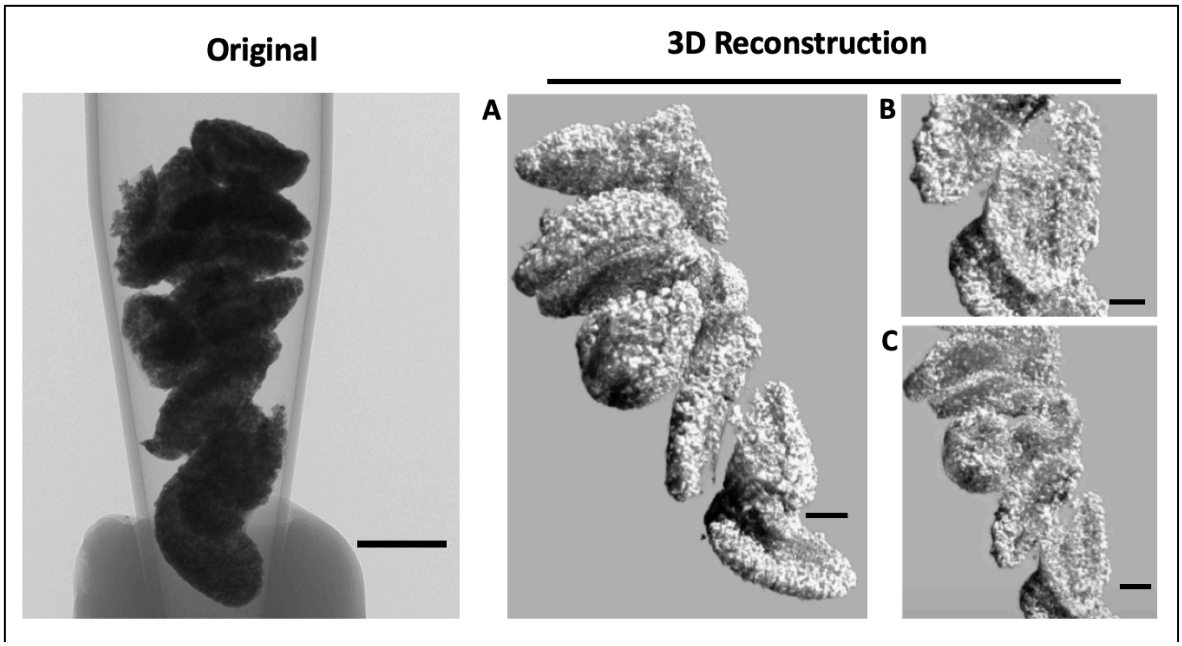

Figure 16: MicroCT Image of a microtube containing particles. The images show the piled particles which create free spaces in between. Left) Original image of particles in a microtube. Right) 3D full reconstruction of the particles. A) Particle's porosity is shown. B) Zoom-in on the particles' porosity. C) Zoomed transversal cut on the reconstructed image of the particles. Left) Scale 1 mm. A, B, C) Scale 0.5 mm.

The results show that the weight of the particles on the top do not interfere with the particles before, as it is not observed that any crushing occurs between them. Also, it can be clearly seen that the coating allows for the particle's 3D stabilization and it helps maintain the creation of spaces of air between each particle.

Then, the 2% alginate coated particles were measured for mechanical properties but in groups of 0.5 ml of particles and were compared with the non-coated ones (0%). As elastic modulus and yield strength are intensive properties, the first linear slope of the stress-strain plot was considered as the elastic-like modulus of the grouped particles and the maximum stress of that slope was considered as the yield strength. The following figure shows the average of these two parameters.

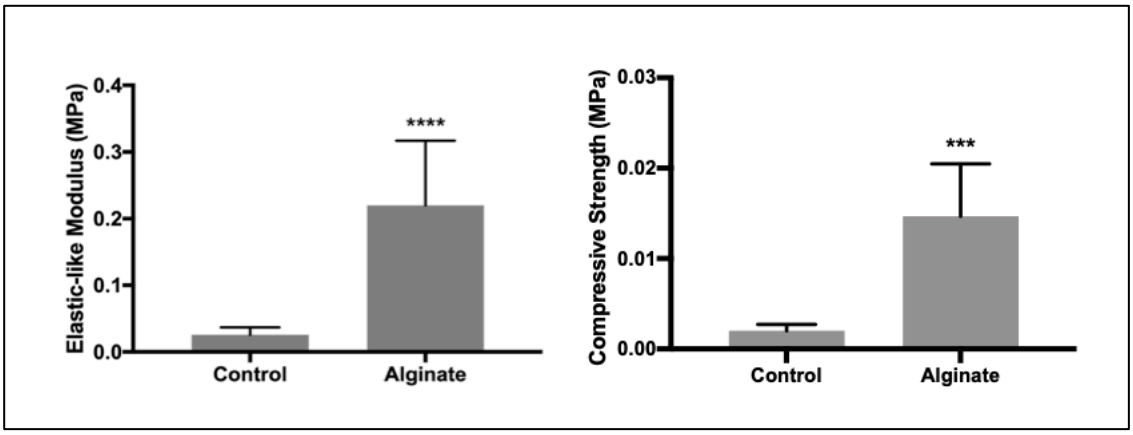

Figure 17: Measurements of mechanical properties of the post-processed particles and their grouped effect. Left) Apparent elastic-like modulus and right) yield strength of grouped particles. Statistical analysis done with Mann-Whitney test(**** $p < 0.0001$, *** $p < 0.001$).

It can be seen that as a group, the mechanical properties of the coated particles were significantly higher than the ones without the coating. However, both groups were much lower than single particle compressive strength.

To summarize the development process of the alginate coating to the 3D printed calcium sulfate particles, a flow diagram was made for illustration purposes (figure 18).

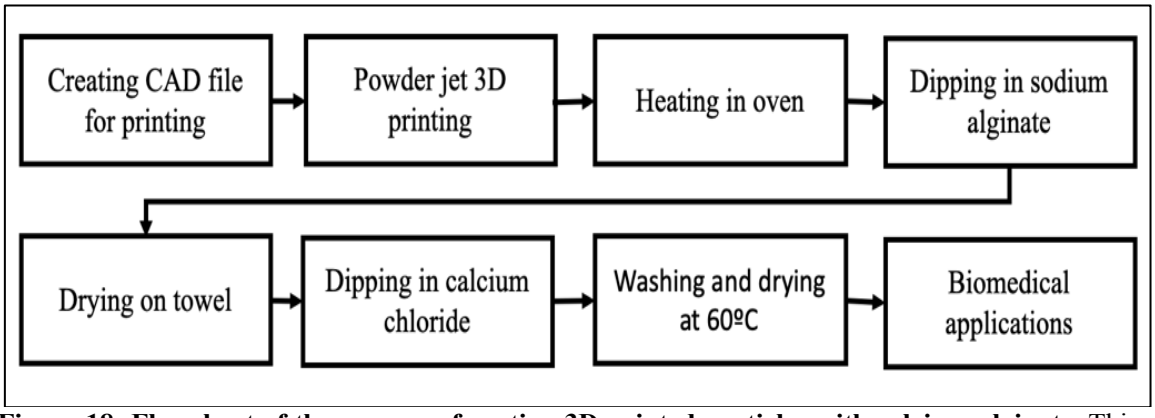

Figure 18: Flowchart of the process of coating 3D printed particles with calcium alginate. This includes the cross-linking step with calcium chloride.

It can be noted that the process should be carried out after the printing of the desired object is done. Thus, not interfering with the printing process itself. The biomedical application step should include previous sterilization.

4.10 Cell viability and toxicity assays

The component 2,3-bis(2-methoxy-4-nitro-5-sulfophenyl)-5-[(phenylamino)carbonyl]-2H-tetrazolium hydroxide (XTT), is used as an indicator for cell metabolic activity which implies cell viability (Freshney, 2005). XTT is metabolically reduced in active cells to a formazan product which is soluble in water and in the cell medium. This reagent can be read with a microplate reader at a specific absorbance without further processing of the sample, therefore eliminating a solubilization step and shortening the assay procedure (Scudiero, 1988). Tetrazolium assays can also be useful for measuring the effects of different substances on cell growth, like drugs, hormones or toxins and in the case of this work, the effects of the alginate-calcium sulfate composite on cell cultures (Paull, 1988).

As a result of using this cell viability assay, there exists a 20% and 10% decrease of XTT metabolism at 24 and 48 hours respectively, when compared to the control condition. This difference is significant at 48 hours in two of the independent experiments. At 24 hours the independent experiments do not show a significant difference due to the data variability. However, when taking the three replicates into consideration, there is a significant different of both conditions (24 and 48 hours) with the control condition.

Cytotoxicity can be defined as cell death caused by external agents. The main advantages of cytotoxicity assays are the speed, reliability and simplicity of the evaluation as it uses absorbance to quantify the amount of LDH that is left in the medium and does not require animal testing. (Decker *et al.,* 1988). This is a common assay for cytotoxicity as it is widely used in *in vitro* toxicology. We can express cytotoxicity as the amount of LDH that is leaked in the supernatant. This is because when irreversible cell death occurs, the plasma membrane breaks and allows LDH to leak out of the cell into the culture medium (Fotakis *et al.,* 2006). It can be observed by the results that the positive control (0 hours) shows a small basal percentage of LDH release from the cells (about 7% compared with

the death control). This effect seems to be maintained in the 3 replicate experiments with only a 1-2% increase at 24 and 48 hours. When plotting the average of the 3 experiments, there is no significant difference between conditions (figure 19).

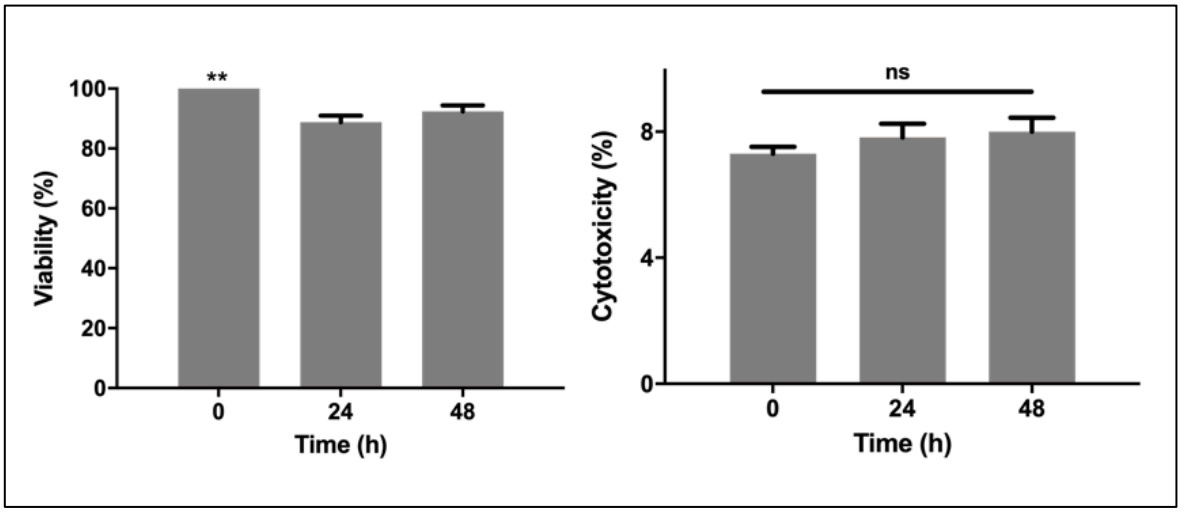

Figure 19: Cell viability and cytotoxicity of NIH/3T3 after incubation with the alginate coated particle. Left) Viability quantification in relation to the death control (100%). Right) Cytotoxicity quantification (%) of the samples. Each figure represents the three independent experiments. Statistical significance was determined through ANOVA test and multiple comparison was performed using Bonferroni test (**$p < 0.01$). Plots courtesy of MSc. David Ñecuñir.

In order to observe the viability of the cells incubated with the coated particle, calcein AM and PI staining were performed. Live cells can be observed in green due to intracellular enzymes (cytosolic esterases) being able to transform the reagent calcein AM into a fluorescent product (Sadeh *et al.,* 2016). The reagent is able to cross the cell membrane while the cells are alive (Bratosin *et al.,* 2005). In addition, dead cells can be observed using the fluorochrome propidium iodide. Propidium iodide (PI) can easily enter the cells once they die because of membrane rupture. This way the fluorochrome is able to bind and label the cell's DNA, located in the now accessible nucleus, allowing it to be seen under a microscope in the color red (Riccardi *et al.,* 2006).

Green cells indicated that the cells had an active metabolism, inferring they were alive. Dead cells were indicated in red. In figure 20, we can observe a representative image of

each condition (cells with the coated particle at 24 and 48 hours, live cells and dead cells). We can observe a few red dyed cells which match with the XTT decrease results on the 48hr. condition. However, this number is very similar to the positive control (at 0 hours).

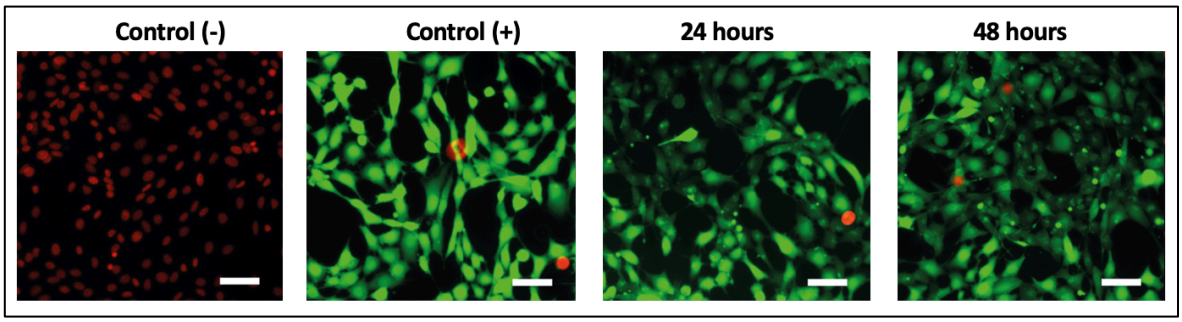

Figure 20: Propidium iodide and calcein AM assay of cells. From left to right, negative control (total cell death), 0 hours, 24 hours and 48 hours after implantation of particle. Scale 50 µm. Images courtesy of MSc. David Ñecuñir.

4.11 Zebrafish larvae toxicity assay

The experiment showed no death of zebra fish larvae when incubated with the particle at both times (24 and 48 hours) (figure 21, right). In fact, all the 10 larvae from each well had similar heartbeat rates as the control (larvae without particles at 48 hours) when observed through the microscope. Also, no signs of morphology changes or development damage were observed (figure 21, left).

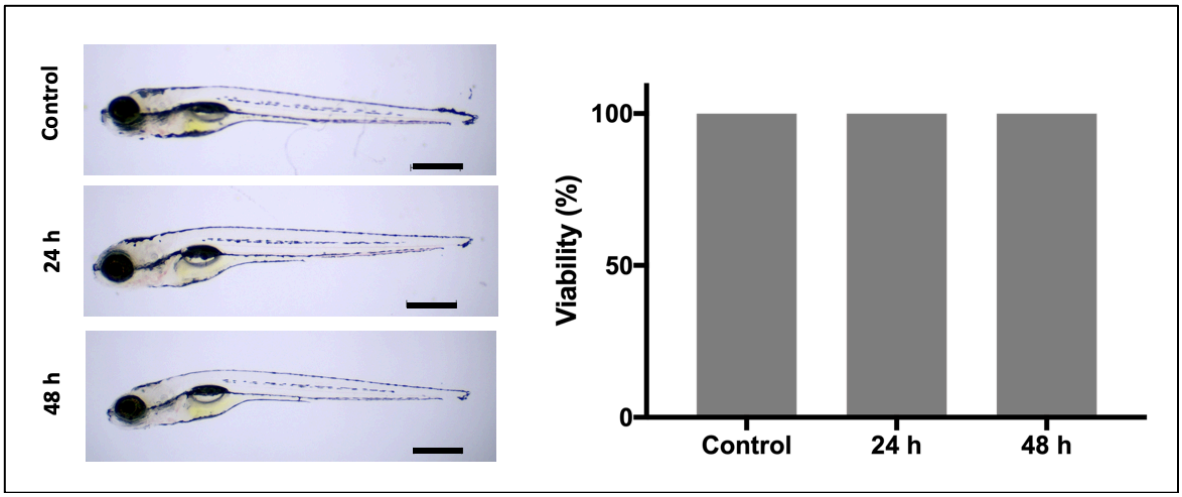

Figure 21: Viability and toxicological assay *in vivo* using zebra fish larvae. Left) Zebra fish after 24 hrs. and 48 hrs. of exposure to post-processed particles. Right) Viability measurements compared to positive control (larvae with E3 medium) (N=1, n=3). Scale 250 μm. Images courtesy of Miguel Miranda.

5. DISCUSSION

In this work we were able to develop and evaluate an alginate coating process in 3D printed calcium sulfate particles. The developing of the alginate coating was inspired by the work of Hornyák *et al*. (2017), who created a protocol to coat seeds. In this work the protocol was adapted successfully to the characteristics of the calcium sulfate particles. Then, different physical tests were applied to characterize and compare processed and non-processed particles, resulting in improved mechanical and physical properties for the processed ones. Finally, *in vitro* and *in vivo* viability toxicology assays were performed in order to ensure a basic degree of biocompatibility.

5.1 3D printing, ion exchange and alginate coating.

Another step of sintering could have been applied in order to increase the mechanical properties of the calcium sulfate particles. Ceramics require extremely high temperatures to be sintered (1400 ºC) and naturally have lower densification capacity compared to metals, infiltrating ceramics with metals is a common strategy used to stabilize particles (Mostafaei *et al.,* 2020). This however was going against the biocompatibility objectives that was planned to be achieved in this work.

The possible explanation for the particles dissolving in the ion exchange process is that the solution's viscosity was very low to prevent them from dissolving. This is consequent with the work of Lowmungkon *et al.* (2007) as they described that heating at 300 ºC for 20 minutes did turn particles to be dissolved in the liquid. Also, they tested a bigger and more dense shape, which was not dissolved at greater pre-heating temperatures but it changed color after high temperatures. Moreover, even though the chemical composition was not tested to see how much hydroxyapatite was created, the process did not serve the purpose of improving physical properties and so it was discarded.

It can be noticed that this process only consider a few additional steps after the regular 3D printing process, allowing it to be easily adapted for other powder objects that have been 3D printed (like tricalcium phosphate and hydroxyapatite). It also important to report that the process is handmade and the resulting particles may vary accordingly to the

performing scientist. It is of great advantage as for further investigation to automatize this manual process that will ensure greater replicability.

5.2 Mechanical testing

The stress-strain curves that were obtained had an initial linear curve, a plateau and then an exponential phase, which are consistent with previous works on porous scaffold structures (Hoque *et al.,* 2009). Results of single particle mechanical tests showed an increase of the elastic modulus and yield strength on the 2% alginate coated particle. Also, the consistency of the 2% alginate was found easily to handle when making the particles. Thus, this group of particles was chosen to continue on the physical tests. Variations of results can be explained by the shape of the particles, as they are convex it does not stay always in the same position in order to compress them in the exact same manner. Moreover, there is variation of size in the fabrication of the particles as the 3D printing process does not make exact replicates for smaller sized objects. Even if the results were positive for testing the hypothesis of this work, there is difference on the magnitude of the elastic modulus with other synthetic bone grafts. For example, calcium sulfate in powder form has a compressive strength of 23 MPa (Moore *et al.,* 2001) and in the case of the geodesic 2% alginate-coated particle it was around 0.5 MPa. Elucidating that the shape and thinness of the particle plays a big role on the mechanical properties and to compare the values with other bone grafts it would require to have similar shaped particles.

With the information on Figure 17 about the mechanical properties of the group effect, we can state that the particle increases its mechanical properties after being coated with calcium alginate. We can notice that when measuring mechanical properties on group of particles the numbers were much lower than single particle tests. This might be caused due to the presence of more air space in between particles, creating an apparent porosity if the material is taken as a whole and lowering its mechanical properties (like elastic modulus) when the porosity is higher (Lu *et al.,* 1999). There could also be a sliding and accommodation effect between particles during the compression test that could account for the decrease in magnitude.

5.3 Physical characterization

Solubility testing elucidated how the polymeric coating can prevent the particle from dissolving completely in physiological solutions and thus preventing early degradation of the calcium sulfate particle (figure 12 and 13). Even if it did release a fair amount of calcium sulfate in the medium after 7 days, it was 70% less than without the alginate coating and the particle did hold the original shape. The release of calcium sulfate might probably be from the coating not being 100% hermetical and thus, a small defect on the coverture can make the calcium sulfate leak, which is also shown in figure 9. One study shows that doing a double coating with alginate, can prevent leakage of the inner product (UEMURA *et al.,* 2000). This can be of great advantage as a study showed that smooth implant surfaces are recommended because they can diminish the probability of bacterial adhesion (implying infection) but it does not affect significantly the amount of cell adhesion, improving its qualities for tissue applications (Richards *et al.,* 1996).

In figure 15, the great difference in weight can be explained by the alginate capacity to absorb large amounts of water as it is a hydrogel and water gets easily retained on its matrix. The swelling of this material is something to pay attention when using it for tissue implantation as it could soak more medium that it was intended. One way to mitigate this effect is to pre-soak the particles in physiological medium before applying in a defect.

It must be noticed that the process does allow for some extra parts of alginate hanging from the sides as the process is not automatized and depends greatly on human experience and care. It can be avoided allowing the particle to rest more time in the paper towel or developing an automatized protocol for coating which may include vacuum drying. This will ensure less variability in most of the tests previously performed.

5.4 *In vitro* and *in vivo* viability and toxicology assays

The LDH assay suggests that cells incubated with the coated particle does not present a major cytotoxic risk in terms of damage and permeability because their values are close to basal levels. However, we can see a slightly decrease in cellular division rate at both

times (24 and 48 hours), showed through XTT metabolism. Observing at the calcein AM and propidum iodide staining (figure 20), we can infer that the few dead cells that are seen at 0 hours might be related to the presence of organic components of the particle during the printing process. This is normally taken away from the material after curing, but a study shows that it should be cure at higher temperatures (1125 ºC) to completely remove the organic components of the printed particles (Asadi-Eydivand *et al.,* 2016). The XTT results where a small decrease on cellular metabolic activity (in this case, viability) was observed, can imply that initially the particle did cause a decrease on metabolic activity but it did not keep on decreasing after 24 hours. From this we can infer that the particle is not toxic to cells but it can cause slight cell viability decrease when implanting it. It should be noted that at all times cell viability is over the 70% cell viability cutoff imposed by ISO and so the material can be considered as biocompatible (ISO, 2012). Thus, the alginate coated particles are not only non-toxic but also biocompatible with cells.

Further studies on the post-processed particle conclude that not only it is biocompatible but also, cell attachment was observed (appendix 1). Different types of images can show the filopodia extending on the particle's surface. Under the SEM, we can see a high resolution image of a stretched cell indicated with the black arrow. The confocal microscopy image shows the actin fibers (dyed in green) stretching and in contact with other cells. The particles can be seen in dark blue on the back and under the cells. It can be noted that in the 3D reconstruction of the cells, the shape of the cells is not as stretched as in the SEM images; this might be due to the high confluence of cells or the 3D reconstruction itself. However, the cells do not seem to form spheres which is what they would have looked like, if they were not adhered to the surface of the particle. These results are of great relevance as cell attachment is important for tissue regeneration and these results imply that the post-processed particles can be used as bone grafts.

It is inferred by the results of the zebrafish larvae experiment that the alginate coated particles do not release toxic components to the media and thus, are biocompatible to this particular *in vivo* model. These result agree with previous studies of alginate and calcium sulfate toxicity that were tested separately (De Vos *et al.,* 1997). Other, more specific

parameters could be tested in the future like edema formation, head-trunk angle, swim bladder development, etc. as other works in zebrafish larvae toxicology testing have done (Alvarez *et al.,* 2018). Moreover, it is to be noted that this experiment corresponds to only one biological replicate and it would be desirable for the near future to repeat the experiment with other groups of zebrafish larvae. These results allow for further research as a bone graft in larger animal or phase I human studies.

6. CONCLUSIONS AND PERSPECTIVES

Alginate covered non-toxic calcium sulfate particles were successfully obtained, allowing their stabilization and improving their mechanical properties. First, the work proved that an alginate hydrogel coating can be applied to the particles unlike other thermionic treatments like ion exchange with ammonium phosphate. The alginate coating at 2% alginate did however increase its original surface in about 20% but it was able to maintain the general shape of the particles. The alginate coating made the particle stable in water solutions like a physiological buffer solution (PBS) at 37 ºC for at least one week. Moreover, after the processing with alginate, the calcium sulfate particle allowed swelling and was able to absorb water increasing its weight in 258%. This is of special relevance for scaffold applications as it could absorb physiological solutions in situ.

Regarding mechanical properties, the dried alginate coating made the original particle stiffer as it increased its elastic moduli and yield strength, respectively. When evaluated in groups of particles, it was observed that the coated particle group was also more resistant to the force applied than the non-coated ones but it was observed a decrease in the magnitude of the stress applied comparing it to the single particle properties. This might be explained by the arrange of the particles and the free spaces of air in between them, which accounts for sliding among them.

Moreover, viability and toxicity were measured in different models. First, particles were co-cultivated with standard mouse fibroblasts (NIH/3T3) cells in order to observe cell viability and toxicity of the resulting process. The results of the different experiments performed showed that the resulting particle was not toxic to the cells but it did show a small decrease on cell viability, probably because of the sensitivities of the different assays. These numbers on viability however are higher than 70% for all conditions, following the guidelines of ISO for considering it a biocompatible object. Lastly, viability was tested in zebrafish larvae model, where it was observed that the oral delivery of the

particle residues did not affect the larvae viability and there were no macroscopic changes in their development and morphology.

Even though this work tested for most of the properties necessary for a mechanically stable and biocompatible bone scaffold, it opens the questions of further research on the particles regeneration process and the possibilities of adding different components to the alginate coating to boost the regeneration and healing properties the particles could have, such as the addition of vascularization factors, osteoblast differentiation proteins, antibiotics, etc. As it was studied before for other ceramic antibiotic carriers, which proves the efficacy of infection treatment (Ferguson *et al.,* 2017).

Additionally, this work allows for further mechanical characterization of the cells adherence forces with the alginate-coated particles using AFM techniques and other atomic and molecular level testing like x-ray diffraction or molecule content. As it would be of interest to study how much these properties change when using different polymers on the particles.

REFERENCES

Abasalizadeh, F. M. (2020). Alginate-based hydrogels as drug delivery vehicles in cancer treatment and their applications in wound dressing and 3D bioprinting. Journal of biological engineering., 14(1), 1-22.

Aldemìr, B. D. (2015). Development, 3D printing and characterization of calcium sulfate based scaffolds for bone tissue engineering. . 19th National Biomedical Engineering Meeting (BIYOMUT) IEE, 1-4.

Allen, S. M. (2000). Three-dimensional printing of metal parts for tooling and other applications. Metals and Materials, 6(6), 589-594.

Alvarez, M. C. (2018). A novel in vivo model to study impaired tissue regeneration mediated by cigarette smoke. Scientific reports, 8(1), 1-12.

Asadi-Eydivand, M. S.-H. (2016). Structure, properties, and in vitro behavior of heat-treated calcium sulfate scaffolds fabricated by 3D printing. PloS one, 11(3), e0151216.

Boyan, B. H. (1996). Role of material surfaces in regulating bone and cartilage cell response. Biomaterials, 17(2), 137.

Bratosin, D. M. (2005). Novel fluorescence assay using calcein-AM for the determination of human erythrocyte viability and aging. Cytometry Part A: the journal of the International Society for Analytic Cytology, 66(1), 78-84.

Burg, J. P. (2000). Biomaterial developments for bone tissue engineering. 21, 2347-2359.

De Vos, P. D. (1997). Effect of the alginate composition on the biocompatibility of alginate-polylysine microcapsules. Biomaterials, 18(3), 273-278.

Decker, T. &.-M. (1988). A quick and simple method for the quantitation of lactate dehydrogenase release in measurements of cellular cytotoxicity and tumor necrosis factor (TNF) activity. Journal of immunological methods, 115(1), 61-69.

DeGroot, J. (1998). Carriers that concentrate native bone mor- phogenetic protein in vivo. Tissue Eng., 41, 4-337.

Enneti, R. K. (2018). Sintering of WC-12% Co processed by binder jet 3D printing (BJ3DP) technology. nternational Journal of Refractory Metals and Hard Materials, 71, 28-35.

Felfel, R. M.-A. (2019). Structural, mechanical and swelling characteristics of 3D scaffolds from chitosan-agarose blends. Carbohydrate polymers, 59-67.

Ferguson, J. D. (2017). Ceramic biocomposites as biodegradable antibiotic carriers in the treatment of bone infections. Journal of bone and joint infection, 2(1), 38-51.

Fotakis, G. &. (2006). In vitro cytotoxicity assays: comparison of LDH, neutral red, MTT and protein assay in hepatoma cell lines following exposure to cadmium chloride. Toxicology letters, 171-177.

Freshney, R. I. (2005). Culture of animal cells: a manual of basic technique. Wiley.

Hollinger, J. B. (1986). Biodegradable bone repair materials. Clin Orthop Rel Res, 207-290.

Hollinger, J. S. (1997). Macrophysiologic roles of a delivery system for vulnerary factors needed for bone regeneration. . Ann New York Acad Sci, 831.

Hoque, M. E. (2009). Processing of polycaprolactone and polycaprolactone-based copolymers into 3D scaffolds, and their cellular responses. . Tissue Engineering Part A, 3013-3024.

Hornyák, I. C. (2017). Sustained Release of a Biodegradable Alginate Coating Covering Chemically Unbound Gentamicin on Human Bone Allograft; And a Method for Colorimetric Drug Release Measurement. SOJ Pharm Sci., 1-6.

Ingaglio, J. F. (2019). Material characteristics of binder jet 3D printed hydrated CSA cement with the addition of fine aggregates. Construction and Building Materials, 206, 494-503.

International Organization for Standardization (2012). Biological evaluation of medical devices. Part 12: Sample preparation and reference materials (ISO 10993-12:2012). Retrieved online from: https://www.iso.org/standard/53468.html

Inzana, J. A. (2014). 3D printing of composite calcium phosphate and collagen scaffolds for bone regeneration. Biomaterials, 35, 4026-34.

Khan, S. N., Tomin, E., & Lane, J. M. (2000). Clinical applications of bone graft substitutes. *Orthopedic Clinics*, *31*(3), 389-398.

Kumar, Y. N. (2013). Calcium sulfate as bone graft substitute in the treatment of osseous bone defects, a prospective study. Journal of clinical and diagnostic research:, 7(12), 2926.

Langer, R. V. (1993). Tissue engineering. Science, 920-6.

Lanza, R., Langer, R., Vacanti, J. P., & Atala, A. (Eds.). (2020). *Principles of tissue engineering*. Academic press.

Laurencin, C. K.-A. (2006). Bone graft substitutes. Expert review of medical devices, 3(1), 49-57.

Lee, K. Y. (2001). Hydrogels for tissue engineering. Chemical reviews, 101(7), 1869-1880.

Lowmunkong, R. S. (2007). Transformation of 3DP gypsum model to HA by treating in ammonium phosphate solution. Journal of Biomedical Materials Research Part B: Applied Biomaterials, 80(2), 386-393.

Lu, G. L. (1999). Mechanical properties of porous materials. Journal of Porous Materials, 6(4), 359-368.

Martina, M. &. (2007). Biodegradable polymers applied in tissue engineering research: a review. Polymer International, 56(2), 145-157.

McGrath, P. &. (2008). Zebrafish: a predictive model for assessing drug-induced toxicity. Drug discovery today, 13(9-10), 394-401.

Mikos, A. G. (1994). Preparation and characterization of poly(L-lactic acid) foams. Polymer, 1068.

Moore, W. R. (2001). Synthetic bone graft substitutes. ANZ journal of surgery, 71(6), 354-361.

Mostafaei, A. E. (2020). Binder jet 3D printing–Process parameters, materials, properties, and challenges. Progress in Materials Science, 100707.

Olivier, A. G. (2012). Cytotoxicity of seven recent dentine bonding agents on mouse 3T3 fibroblast cells.

Pape, H. C. (2010). Autologous bone graft: properties and techniques. Journal of orthopaedic trauma, 24, S36-S40.

Park, H. K. (2009). Shear-reversibly crosslinked alginate hydrogels for tissue engineering. Macromolecular bioscience, 9(9), 895-901.

Parng, C. (2005). In vivo zebrafish assays for toxicity testing. 8(1), 100-106.

Paull, K. D. (1988). The synthesis of XTT: A new tetrazolium reagent that is bioreducible to a water-soluble formazan. Journal of Heterocyclic Chemistry, 25(3), 911-914.

Pawar, S. N. (2012). Alginate derivatization: a review of chemistry, properties and applications. Biomaterials, 33(11), 3279-3305.

Rajesh, R. R. (2017). Alginate in Bone Tissue Engineering. In Seaweed Polysaccharides, Elsevier., 349-368.

Ratner, B. D., Hoffman, A. S., Schoen, F. J., & Lemons, J. E. (2004). *Biomaterials science: an introduction to materials in medicine*. Elsevier.

Riccardi, C. &. (2006). Analysis of apoptosis by propidium iodide staining and flow cytometry. Nature protocols, 1(3), 1458.

Richards, R. G. (1996). The effect of surface roughness on fibroblast adhesion in vitro. Injury, 27.

Sadeh, N. O.-B. (2016). Acute live/dead assay for the analysis of toxic effects of drugs on cultured neurons. Bio-protocol, 6(15), e1889-e1889.

Scudiero, D. A. (1988). Evaluation of a soluble tetrazolium/formazan assay for cell growth and drug sensitivity in culture using human and other tumor cell lines. Cancer research, 48(17), 4827-4833.

Severino, P. C. (2015). Sodium alginate-cross-linked polymyxin B sulphate-loaded solid lipid nanoparticles: Antibiotic resistance tests and HaCat and NIH/3T3 cell viability studies. Colloids and Surfaces B: Biointerfaces, 129, 191-197.

Tsuruga, E. T. (1997). Pore size of porous hydroxyapatite as the cell-substratum controls BMP-induced osteogenesis. The Journal of Biochemistry, 121(2), 317-324.

UEMURA, Y. H. (2000). Effect of calcium alginate coating on the performance of immobilized yeast cells in calcium alginate beads. Chemical Engineering Communications, 177(1), 1-14.

Venkatesan, J. N. (2014). Role of alginate in bone tissue engineering. Advances in food and nutrition research, 73, 45-57.

Wang, L. S. (2003). Evaluation of sodium alginate for bone marrow cell tissue engineering. Biomaterials, 24(20), 3475-3481.

APPENDIX

Appendix 8.1: Cell adhesion to the post-processed particles.

As it was observed that the alginate coated particle was not toxic to the cells, we evaluated the cells adherence to the particle, as its going to be useful in biomedical application as scaffolds. In Appendix 1, we can notice adherence by the extended stretching of filopodia in the particle's surface. If the cells were not adhered, then we would see circular cell shapes.

To confirm cellular adhesion, the cell's actin fibers and nucleus were dyed and images were taken with an epifluorescence microscope. The cell's actin fibers can be seen on top of the particle which seem less stretched as the ones in the SEM imaging, this might be due to the high confluence of cells. The blue signal of the nuclei cannot be seen clearly due to the noise made by the particle's self-fluorescence. It can be observed in blue to which part of the internal side of the particles the cells adhere to but due to the size of the particle it is not seen completely.

In order to observe cellular adhesion and morphology over the particles, NIH/3T3 cells were seeded in a 24-well microplate, where 4 particles were previously placed on the bottom of the wells. The microplate was kept in the incubator for 2 days. The cells were then fixed for 4 days. Then, the cells were dehydrated and covered with a gold coating. Images were taken with a scanning electron microscope Hitachi TM3000 (Hitachi High Technologies Inc., Tokyo, Japan) and processed using the software provided by the brand at the Advanced Microscopy Unit from Pontificia Universidad Catolica de Chile. In order to visualize the nucleus and actin fibers, Hoechst and Phalloidin 488 assay were performed to the cells adhering to the particle. For this, cells were seeded over a 24-well microplate well containing 4 coated particles (2% alginate) for 2 and 7 days. They were and permeabilized. Then, they were washed and incubated with Phalloidin 488 dye and Hoechst 33342 Stain Solution. They were mounted in a glass cover. Images were taken with an inverted confocal microscope (Zeiss LSM 880 with Airyscan detector).

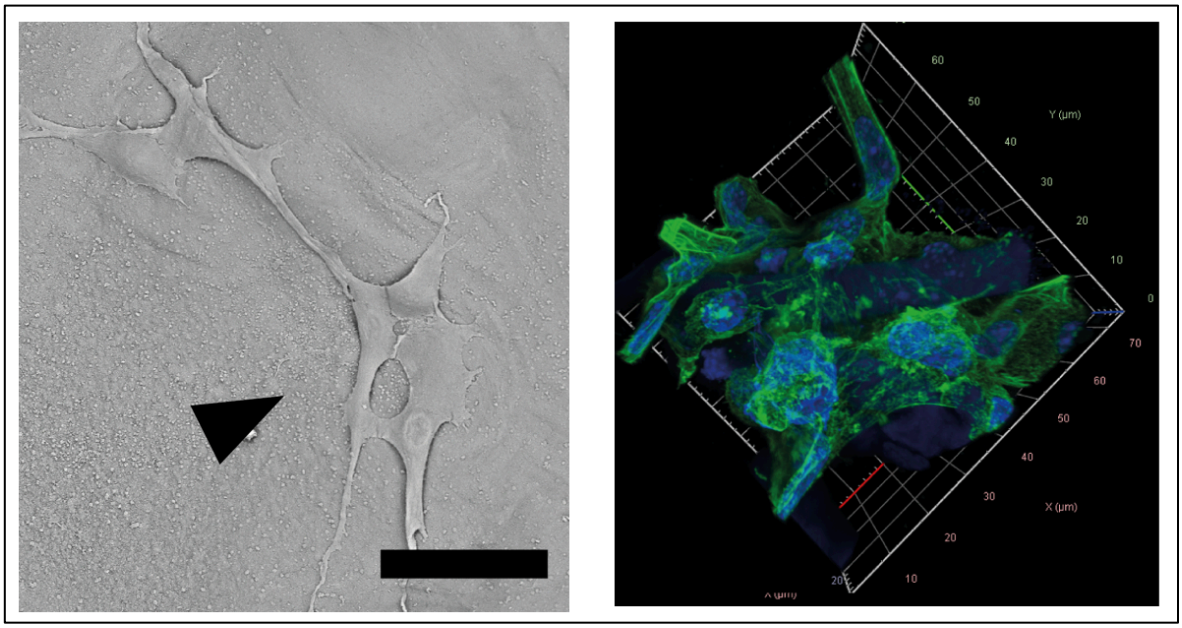

Appendix 1. Cell adhesion experiments of the post-processed particle using NIH/3T3 cell line. Left) SEM image of cells cultivated over alginate coated particle. Arrow indicates a cell being attached to the particle's surface (2% alginate). Right) 3D reconstruction of epifluorescence microscopy images. Cells were cultivated at high confluence over the particle. Left image scale is 50 µm. Images and experiment courtesy of Dr. Jovita Besa and MSc. David Ñecuñir.